Origin of the High work function and high conductivity of MoO_3

Yuzheng Guo, John Robertson
Engineering Department, Cambridge University, Cambridge CB2 1PZ, UK

The large work function of MoO_3 of 6.6eV is due to its closed shall character and the dipole layer created by planes of terminal O_1 oxygen sites which lower the electrostatic potential of the inner Mo-O units. These O_1 sites arise from the high stoichiometry of MoO_3. The O vacancy is most stable at the 2-fold O_2 site. It is a shallow donor and has a small formation energy in the O poor limit, so that MoO_3 easily becomes a degenerate semiconductor.

The work functions of elemental metals range from 2.14 eV for Cs to 5.65 eV for Pt [1]. The possibility that metallic conductors could have work functions 1 eV larger than Pt is extremely valuable. The most well known of these is MoO_3 [2-8] and others are WO_3, CrO_3 and V_2O_5 [8]. These materials are transparent, wide-gap semiconductors that can be degenerately doped by defects. MoO_3 is a layered oxide also used as a dehydrogenation catalyst, Li battery electrode, supercapacitor electrode and electrochromic material [3-5]. Due to its high work function, MoO_3 is now being intensively studied as a transparent anode and hole transport layer for organic light emitting diodes (OLEDs) and organic photovoltaics (OPVs) [6-12], and as an anode or hole transfer dopant for graphene and MoS_2 devices [10-15]. Given its high work function, band gap and defect induced conductivity, it is important to understand how these properties arise. There are several previous calculations of its electronic structure and surface defects, largely motivated by its catalytic properties [17-22], but there has so far been no account of the origin of the unusually large work function or its conduction properties. The oxides are all closed shell oxides from the middle of the transition metal series. We show that the high work function arises from its closed shell properties plus a dipole layer on surface of each layer, as a structural consequence of the high stoichiometry. The high conductivity arises because the O vacancy is shallow and has low formation energy in O-poor limit. This sets the Fermi energy E_F at the conduction band edge.

MoO_3 has two phases in ambient conditions, the β phase as in monoclinic ReO_3 and WO_3 (space group $P2_1/n$), and the thermally stable, orthorhombic α phase with space group P*bmn* [23-24], as used here. The α phase has a layer structure (Fig 1). Each layer consists of a bilayer of Mo atoms, separated by 3-fold O_3 sites in the z direction, 2-fold O_2 sites in the x direction, and terminated by 1-fold O_1 sites on each layer surface. This gives a distorted octahedral site for the Mo atoms. The terminal O_1 sites are inter-digitated between adjacent layers. Fig 1(c) shows a single slice labeling the different O sites.

Here, in order to understand the origin of the large work function and conductive properties, we calculate the bulk electronic structure, electron affinity, and the energy levels and formation energies of the O vacancies. The calculations are carried out in the generalized gradient approximation (GGA) using the CASTEP density functional code, with norm-conserving pseudopotentials for Mo and O generated by the OPIUM method. A plane-wave cutoff energy of 780 eV is used, which converges total energy differences to under 1 meV/atom. Brillouin zone integrations use a Monkhorst-Pack k-point sampling grid which converges the energies of the bulk unit cell to similar accuracy. Geometry optimizations are converged when

forces are below 0.02 eV/ Å. The local density functionals are well known to under-estimate the band gap of semiconductors, which affects predictions of defect levels. We therefore also use the screened exchange (sX) hybrid functional to correct this error [25,26].

Local density functionals also do not describe well the van der Waals (vdW) bonding between layers. Our calculations confirm this for MoO_3. Thus, we included vdW interactions empirically in CASTEP using the DFT-D2 method [27]. The experimental lattice constants of 2.964Å, 3.699 Å, and 12.836 Å are used in the calculations.

Fig. 2 shows the calculated band structure and density of states of α-MoO_3. The calculated band gap is 3.04 eV in sX, close to the experimental value of 3.0-3.3eV [2]. The sX band gap is 1.0 eV larger than the GGA value. The band structure shows that MoO_3 has an indirect band gap. The conduction band minimum (CBM) is along the XS direction while the valence band maximum is at T. The conduction band dispersions differ slightly from the GGA results of Scanlon [22], who found the CBM to lie at Γ. The difference arises because they used the GGA relaxed lattice parameters, whereas we used the experimental ones. It does not arise from the different functional. The partial DOS in Fig 2(b) shows that CBM consists of Mo d orbitals while the VBM consists of O p orbitals. This is because MoO_3 is a standard closed shell d^0 system. The Mo-O bonds are polar, resulting in a large band gap.

We now discuss the large work function of MoO_3. We can evaluate the work function by calculating the electrostatic potential for a supercell of two layers of MoO_3 and 10Å of vacuum. The supercell is extended along the layers, so as to include an O vacancy. The vacancy levels are shallow (see later), which sets the Fermi energy just below the CBM. This allows us to use GGA to calculate the electron affinity without worrying about the band gap under-estimate in GGA. This is helpful because the electrostatic potential is much better defined in GGA than for a hybrid functional. The vacuum level is defined by the flat potential outside the MoO_3 layers. The electrostatic potential is shown in Fig 3(a). E_F is calculated to lie at 6.25 eV below the vacuum level. This is in reasonable agreement with the experimental value of 6.7 eV [2]. The calculated CBM therefore lies at ~6.2 eV below the vacuum level. A reference calculation is carried out for the relaxed (110)1x1 non-polar surface [28] of rutile TiO_2. Mo is +6 while Ti is +4. The edges of the Mo-O layers in MoO_3 are terminated by non-bridging O_1 sites, whereas the TiO_2 slab is terminated by bridging, 2-fold coordinated O_2 sites.

The large work function arises as follows. MoO_3 is a closed shell system, so that the valence band maximum (VBM) consists of O 2p states, which lie ~9.8 eV deep below the vacuum level. The CBM then lies at ~3.1 eV above the VBM. But the VBM in other closed shell systems like TiO_2, SnO_2, or ZnO with 3 eV band gaps is also O 2p-like, but the work function of MoO_3 is 1.5 – 2.0 eV larger than for these oxides [8]. The larger work function arises from two factors in the case of MoO_3. First, the MoO_3 layers have terminal O_1 sites lying on the outside of the layers. The layers are overall neutral, despite being terminated by an anion. They are a type-2 surface in the classification of Tasker [29]. This O-Mo arrangement on the external layer creates an additional dipole layer which lowers the potential inside the layer (determining CBM) to be deeper than in TiO_2.

This is seen in the electrostatic potentials plots of Fig 3(a,b). The potential is averaged into the plane. The potential shows a number of dips at the center of each Mo, O or Ti atom column. Using the atomic structures overlayed on the potential plot, we can see the minima near the O atoms in the MoO_3 or TiO_2 bulk. This potential has a horizontal reference line through it. We then see that the potential on the surface O_2 sites of TiO_2 is 1.09 eV higher, as indicated, because they are on the surface.

On the other hand, for the two MoO_3 layers, we find the potential of the two O_1 sites between the two layers; this is also marked by a horizontal reference line. We compare this to the potential at the external O_1 site, and see that this lies 6.29 eV above the reference potential. In the case of MoO_3, the terminal O_1 sites are creating a very large dipole layer to the MoO_2 planes. The dipoles oppose each other in the center, where the O_1 sites inter-digitate. The dipole layer is poorly screened in the case of MoO_3, so the resulting potential step is large. In the case of TiO_2 (110)1x1, the dipole potential step is smaller, because it is O_2 sites, and the screening is higher, so the potential step is smaller.

Thus, the dipole layer due to the terminal O_1 sites is critical to the large work function. O_1 sites are a structural consequence of the large x3 stoichiometry of Mo to O. The other high work function oxides CrO_3 and V_2O_5 have different structures, but also have the terminal O_1 sites because of the high stoichiometry (as well as the closed shell nature).

The difference between 6.29 eV and 1.09 eV exaggerates the difference in dipole potentials. This is partly due to the atomic pseudopotentials used. Our accurate calculations on MoO_3 for figs 1-2 used a pseudopotential that includes the Mo 4s,4p states in the valence shell, but this would have resulted in a potential diagram with very large fluctuations, distracting from the message. Instead, we used a less accurate pseudopotential in which the Mo 4s,4p states are in the core shell, and only Mo 4d and 5s are valence.

We now consider the high conductivity of MoO_3 and its oxygen vacancy. There are three different O sites in a-MoO_3, having one, two, and three Mo neighbors respectively. We have created an oxygen vacancy at each site and relaxed the structure. The results are shown in Figure 1(d). After relaxation, the 2-fold O_2 vacancy is found to be the most stable, with the same structure in each charge state. Its formation energy is 3.98eV in the neutral state in O-rich conditions in sX. The relaxation of atoms around the vacancy is confined to its own layer; there is no rebonding between layers or other reconstructions. The atoms adjacent to the vacancy do not shift far from their original positions. On the other hand, an O_3 or O_1 vacancy will spontaneously transform into an O_2 vacancy. The energy order is the same as in Ref [19].

The charge transition state for the O vacancy is plotted in Fig. 5. The defect formation energy is calculated in the usual way [36], using a 144 atom 3x2x3 unit supercell. The supercell size is fixed at that of the defect-free cell. The internal geometry is further relaxed within sX, using a single special k-point of (1/4, 1/4, 1/4). The oxygen chemical potential (μ_O) is referred to that of the O_2 molecule, taken as zero, which is the O-rich limit. The O-poor limit corresponds to the experimental MoO_2:MoO_3 equilibrium and is $\mu(O)$ = -1.74 eV. The heat of formation of MoO_3 is -2.66 eV per O atom [37].

The defect formation energy is calculated to be 3.98 eV for the neutral state in O-rich condition, Fig 4(a). The 0/2+ transition lies in the band gap, about 0.3 eV below the conduction band minimum (CBM). This shows that the defect is shallow, which explains the n-type conduction of MoO_3. The 0/2+ transition has a negative-U character. In O-poor condition, the formation energy is lowered by 1.74 eV, fig 4(a). The vacancy formation energy is now 2.16 eV when E_F is at the CBM. The -2 and -1 state touches the 0 line at the CBM, indicating a localized state at the CBM.

The gap state of the 2-fold vacancy is shown in Fig. 4(b). The state is confined to the layer of the vacancy and consists of Mo d_{xz} orbitals of the Mo layer next to the O vacancy. The PDOS for the neutral defect is shown in Fig. 6(b). The defect state is 0.3 eV below the CBM. If we compare the defect Mo PDOS and that of the perfect cell, it is clear that a defect state is shifted down from the Mo d states.

The second factor is that the O vacancy is deep in ZnO and SnO_2, but is a shallow donor in MoO_3. Thus the intrinsic defects of MoO_3 make it a n-type semiconductor, and partially reduced MoO_{3-x} is a degenerate n-type semiconductor. Its large work function means that it transfers *holes* into any adjacent layer of lower work function (like graphene or MoS_2), despite being n-type by itself. This is the basis of present extensive use of MoO_3 and related M^{6+} oxides as hole dopants in 2-dimensional electronics [2,6-15].

In conclusion, MoO_3 is a high electron affinity oxide because of its closed shell character and the dipoles created by its internal layer structure. It can have metallic conductivity because the O vacancy is shallow and is easily formed by partial reduction of MoO_3.

The authors are grateful to EPSRC for funding.

References

1. H B Michaelson, J Appl Phys 48 4729 (1977)
2. M Kroger, S Hamwi, J Meyer, T Riedl, W Kowalsky, A Kahn, App Phys Lett 95 123301 (2009); Organic Electronics 10 932 (2009)
3. S. H. Lee, Y H Kim, R Deshpande, P A Parilla, E Whitney, D T Gillespie, K M Jones, A H Mahan, S Zhang, A C Dillon, Adv. Mater. 20, 3627 (2008)
4. T. Brezesinski, J. Wang, S. H. Tolbert, and B. Dunn, Nat. Mater. 9, 146 (2010).
5. K Chen, S Xie, A T Bell, E Iglesla, J Catal 198 232 (2001)
6. J Meyer, R Khalandovsky, P Gorn, A Kahn, Adv Mat 23 70 (2011)
7. J Meyer, S Hamwi, M Kroger, W Kowalsky, T Riedl, A Kahn, Adv Mats 24 5408 (2012)
8. M T Greiner, M G Helander, W M Tang, Z B Wang, J Qiu, Z H Lu, Nat Mats 11 76 (2012)
9. Z Zhang, Y Xiao, H X Wei, G F Ma, S Duhm, Y Q Li, J X Tang, App Phys Exp 6 095701 (2013)
10. Z. Chen, I Santoso, R Wang, L F Xie, H Y Mao, H Huang, Y Z Wang, D Ma, A T S Wee, W Chen, Appl. Phys. Lett. 96, 213104 (2010);
11. L Xie, X Wang, H Y Mao, R Wang, B Ozyilmaz, K P Loh, A T S Wee, W Chen, App Phys Lett 99 012112 (2011)
12. S L Hellstrom, M Vosgueritchian, R M Stoltenberg, I Irfan, M Hammock, Y B Wang, C Jia, X Guo, Y Gao, Z Bao, Nanolett 12 3574 (2012); J Meyer, P Kidambi, B C Bayer, C Weijtens, A Kuhn, A Centeno, A Zurutuza, J Robertson, S Hofmann, Sci Rep 4 5380 (2014)
13. H Park, P R Brown, V Bulovic, J Kong, Nanoletts 12 133 (2012)
14. C. Battaglia, X Yin, M Zheng, I D Sharp, T Chen, S McDonnell, A Azcati, C Carraro, R M Wallace, A Javey, Nano Lett. 14, 967 (2014)
15. S. Chuang, C Battaglia, A Azcati, S McDonnell, J S Kang, X Yin, M Tosun, R Kapadia, H Fang, R M Wallace, A Javey, Nano Lett. 14 1337 (2014)
16. F Cora, A Patel, N M Harrison, C Roetti, C R A Catlow, J. Mater. Chem. 7, 959 (1997)
17. A Sayede, T. Amriou, M. Pernisek, B. Khelifa, C. Mathieu, Chem. Phys. 316, 72 (2005).
18. M Chen, C M Friend, E Kaxiras, J Chem Phys 112 9617 (2000)
19. R Tokarz-Sobieraj, K Hermann, M Witko, G Mestl, R Schloegl, Surf Sci 489 107 (2001)
20. R. Coquet and D. J. Willock, Phys. Chem. Chem. Phys. 7, 3819 (2005)
21. X. Sha, L. Chen, A. C. Cooper, G. P. Pez, and H. Cheng, J. Phys. Chem. C 113, 11399 (2009); YH Lei, ZX Chen, J. Phys. Chem. C 116, 25757 (2012); H. Ding, K. G. Ray, V. Ozolins, and M. Asta, Phys. Rev. B 85, 012104 (2012)
22. D. O. Scanlon, G. W. Watson, D. J. Payne, G. R. Atkinson, R. G. Egdell, D. S. L. Law, J. Phys. Chem. C 114 4636 (2010)
23. G.Andersson, A. Magneli, Acta Chem. Scand. 4, 793 (1950)
24. P. F. Carcia, E. M. McCarron, Thin Solid Films 155, 53 (1987); H. Sitepu, B. H. O'Connor, D. Li, J. Appl. Cryst. 38, 158 (2005)
25. K Xiong, J Robertson, M Gibson, S J Clark, App Phys Lett 87 183505 (2005)
26. S. J. Clark and J. Robertson, Phys. Rev. B 82, 085208 (2010).
27. E. R. McNellis, J. Meyer, and K. Reuter, Phys. Rev. B 80, 205414 (2009)
28. U Diebold, Surf Sci Rep 48 53 (2003)
29. P W Tasker, J Phys C 12 4977 (1979)
30. Y Guo, J Robertson, Appl. Phys. Lett. 104, 112906 (2014)
31. A Kubaschewski, C B Alcock, 'Metallurgical Thermochemistry', (Elsevier, 1979)

Figure captions

1. MoO_3 structure, viewed along the x and y axis. blue balls = Ta, red balls = O. A single slice is shown in (c) for comparison of the defect sites later. Different O sites are labeled. (d) relaxed O_2 vacancy.
2. Band structure and partial density of states of MoO_3 as calculated by the sX hybrid functional.
3. (a) Line-averaged electrostatic potential of a MoO_3 slab containing a relaxed O vacancy. A 10 Å vacuum layer is inserted as reference. The bulk O_2 vacancy is inserted to set E_F close to the CBM. The work function for MoO_3 is 6.25eV. (b) Local electrostatic potential of TiO_2 rutile slab with non-polar (110)1x1 surface with a smaller surface dipole, for comparison. The slab contains an O vacancy. The calculated work function for TiO_2 is 4.60eV.
4. (a) Defect formation energy of the O vacancy as function of Fermi level, in the O-rich and O-poor condition. (b) The O vacancy orbital.

Fig. 1.

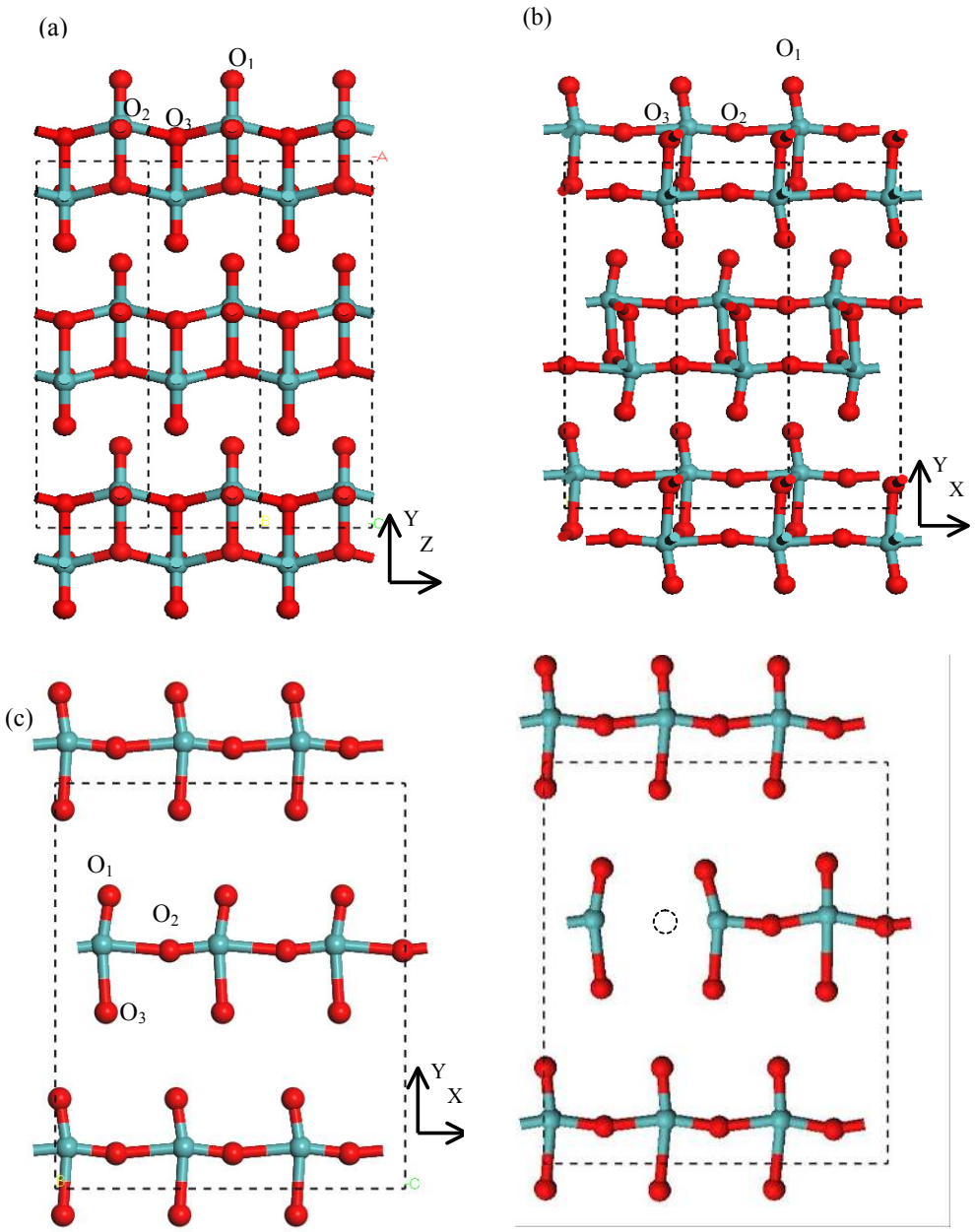

Fig. 2

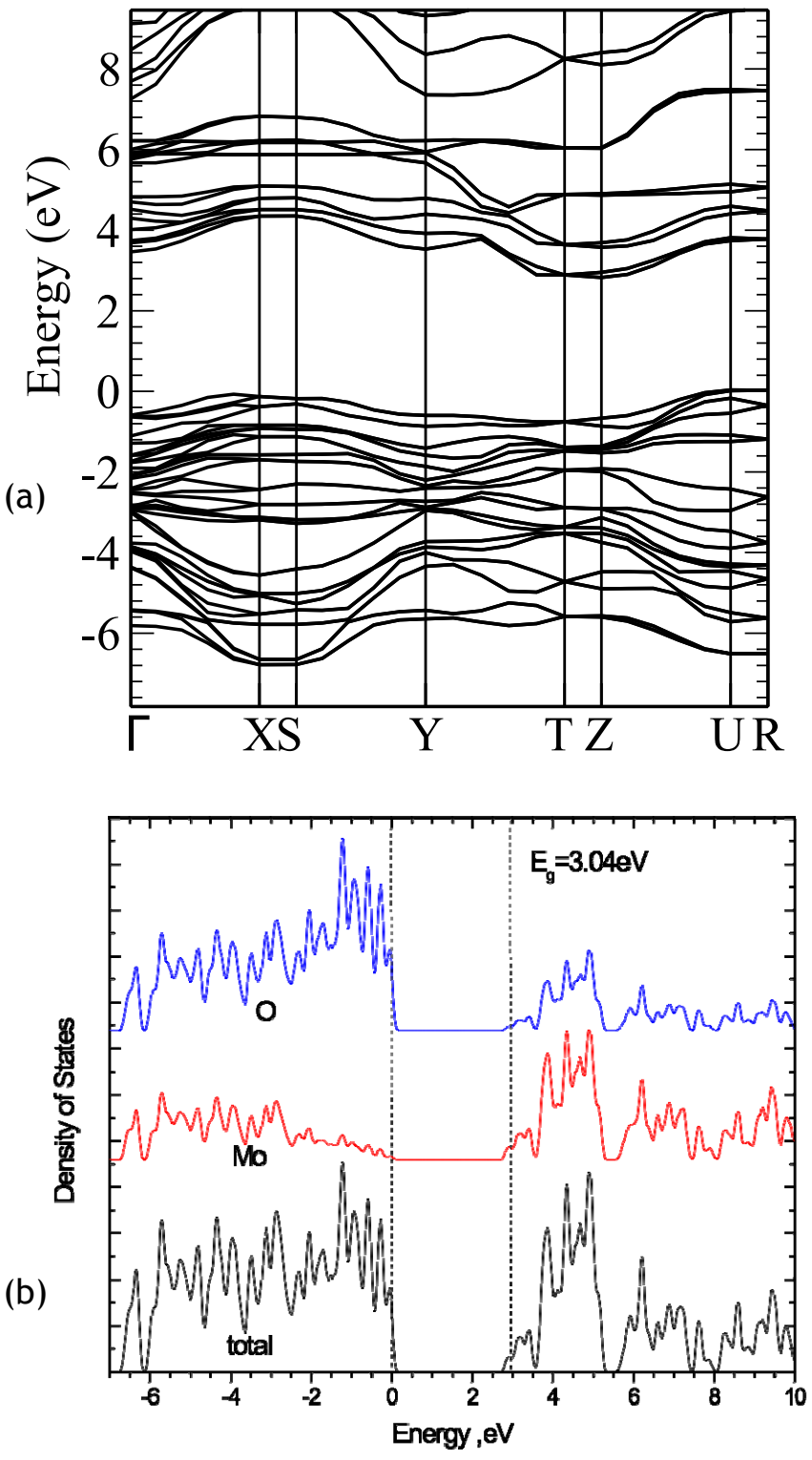
(a)
Energy (eV)
8
6
4
2
0
-2
-4
-6
Γ
XS
Y
T Z
U R
(b)
Density of States
E_g=3.04eV
O
Mo
total
-6
-4
-2
0
2
4
6
8
10
Energy ,eV

Fig. 3.

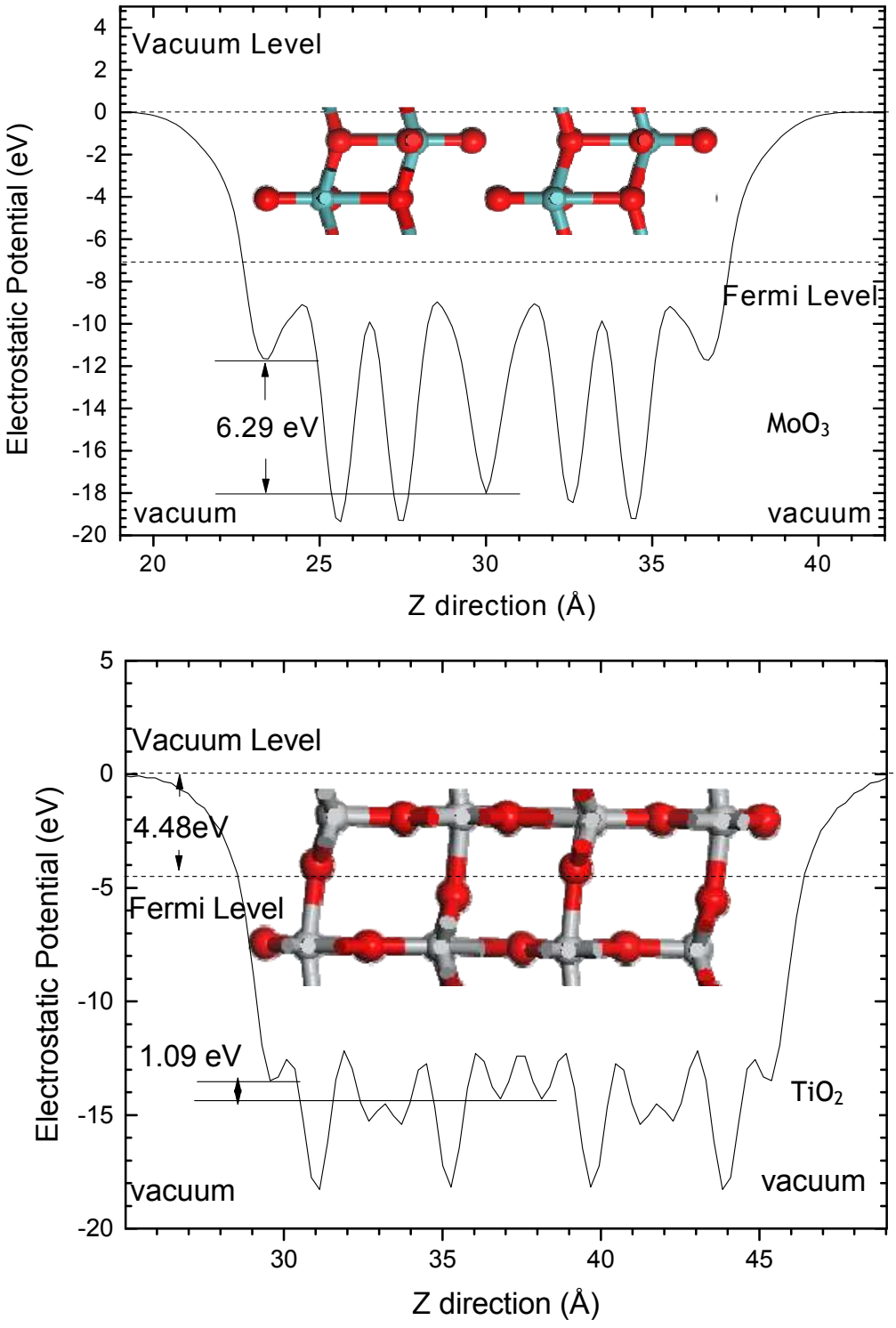
Vacuum Level
Fermi Level
6.29 eV
MoO3
vacuum
vacuum
Electrostatic Potential (eV)
Z direction (Å)
Vacuum Level
4.48eV
Fermi Level
1.09 eV
TiO2
vacuum
vacuum
Electrostatic Potential (eV)
Z direction (Å)

Fig 4

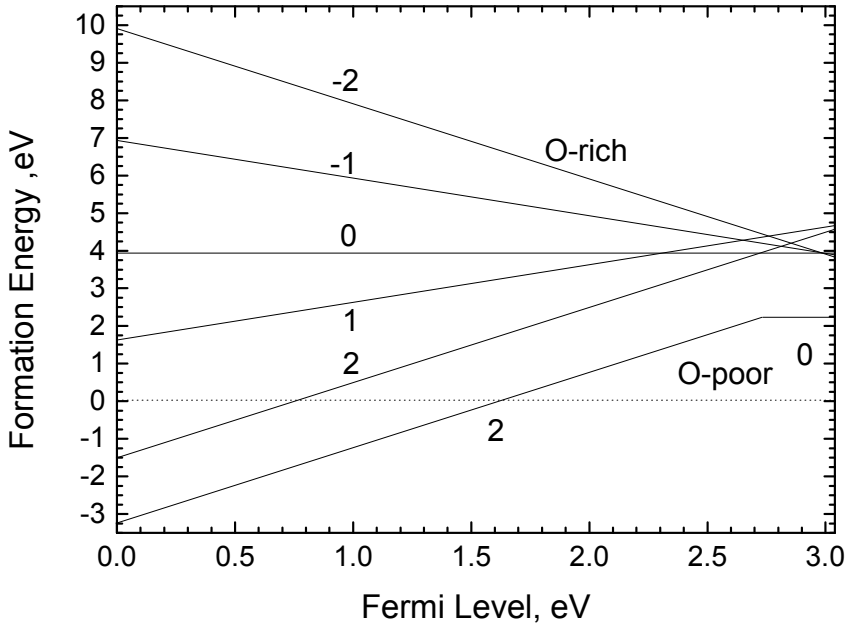

(a)

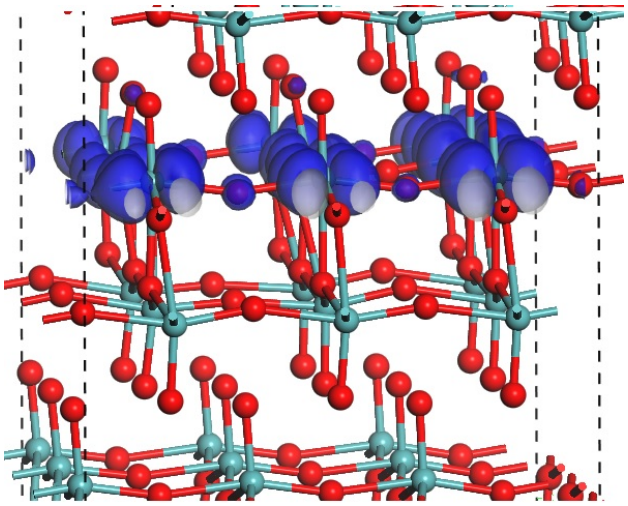

(b)